SARS-CoV-2 ORF6 disrupts nucleocytoplasmic transport through interactions with Rae1 and Nup98

Amin Addetia[1], Nicole A. P. Lieberman[1], Quynh Phung[1], Hong Xie[1], Pavitra Roychoudhury[1,2], Lasata Shrestha[1], Michelle Loprieno[1], Meei-Li Huang[1], Keith R. Jerome[1,2], Alexander L. Greninger[1,2#]

[1]Department of Laboratory Medicine and Pathology, University of Washington, Seattle, Washington, USA

[2]Vaccine and Infectious Disease Division, Fred Hutchinson Cancer Research Center, Seattle, Washington, USA

Running title: SARS-CoV-2 ORF6 disrupts mRNA nuclear export

#Address correspondence to Alexander L. Greninger, agrening@uw.edu

Abstract

RNA viruses that replicate in the cytoplasm often disrupt nucleocytoplasmic transport to preferentially translate their own transcripts and prevent host antiviral responses. The *Sarbecovirus* accessory protein ORF6 has previously been shown to be the major inhibitor of interferon production in both SARS-CoV and SARS-CoV-2. SARS-CoV-2 ORF6 was recently shown to co-purify with the host mRNA export factors Rae1 and Nup98. Here, we demonstrate SARS-CoV-2 ORF6 strongly represses protein expression of co-transfected reporter constructs and imprisons host mRNA in the nucleus, which is associated with its ability to co-purify with Rae1 and Nup98. These protein-protein interactions map to the C-terminus of ORF6 and can be abolished by a single amino acid mutation in Met58. Overexpression of Rae1 restores reporter expression in the presence of SARS-CoV-2 ORF6. We further identify an ORF6 mutant containing a 9-amino acid deletion, ORF6 Δ22-30, in multiple SARS-CoV-2 clinical isolates that can still downregulate the expression of a co-transfected reporter and interact with Rae1 and Nup98. SARS-CoV ORF6 also interacts with Rae1 and Nup98. However, SARS-CoV-2 ORF6 more strongly co-purifies with Rae1 and Nup98 and results in significantly reduced expression of reporter proteins compared to SARS-CoV ORF6, a potential mechanism for the delayed symptom onset and pre-symptomatic transmission uniquely associated with the SARS-CoV-2 pandemic.

Importance

SARS-CoV-2, the causative agent of COVID-19, is an RNA virus with a large genome that encodes accessory proteins. While these accessory proteins are not required for

growth *in vitro*, they can contribute to the pathogenicity of the virus. One of SARS-CoV-2's accessory proteins, ORF6, was recently shown to co-purify with two host proteins, Rae1 and Nup98, involved in mRNA nuclear export. We demonstrate SARS-CoV-2 ORF6 interaction with these proteins is associated with reduced expression of a reporter protein and accumulation of poly-A mRNA within the nucleus. SARS-CoV ORF6 also shows the same interactions with Rae1 and Nup98. However, SARS-CoV-2 ORF6 more strongly represses reporter expression and co-purifies with Rae1 and Nup98 compared to SARS-CoV ORF6. The ability of SARS-CoV-2 ORF6 to more strongly disrupt nucleocytoplasmic transport than SARS-CoV ORF6 may partially explain critical differences in clinical presentation between the two viruses.

Introduction

Control over host protein expression allows viruses to suppress the host's immune response and hijack the host's translational machinery for expression of viral proteins (1–3). Numerous viruses exert translational control by encoding proteins which target nucleocytoplasmic transport, including the nuclear export of host mRNA (4, 5). The host proteins involved in nucleocytoplasmic transport are targets of multiple viruses including vesicular stomatitis virus (VSV), poliovirus, and Kaposi's sarcoma-associated herpesvirus (KSHV) (6–8).

Nup98 is a component of the nuclear pore complex and interacts with the RNA export factor Rae1 to bind single stranded RNA and facilitate the translocation of mRNA through the nuclear pore complex (9, 10). The matrix (M) protein of VSV interacts with the Rae1•Nup98 complex at the nucleic acid binding site to prevent single stranded RNA from binding Rae1•Nup98 (6, 11). As a result, mRNA remains trapped within the nucleus and global gene expression within host cells is significantly reduced (6). A single methionine residue surrounded by acidic residues within VSV M is critical for interactions with Rae1 and mutations at this residue impair VSV M's ability to block mRNA nuclear export (11, 12). ORF10 of KSHV also interacts with Rae1•Nup98 to reduce nuclear export of specific mRNA transcripts (8). Similar to VSV M, ORF10 of KSHV contains a conserved methionine residue surrounded by acidic residues which is likely the interacting motif for the Rae1•Nup98 complex (13).

Severe acute respiratory syndrome coronavirus 2 (SARS-CoV-2), the causative agent of Coronavirus Disease 2019 (COVID-19), is a single stranded RNA virus belonging to the *Betacoronavirus* genus (14). With their large genomes, coronaviruses

including SARS-CoV-2 encode accessory proteins that are not required for viral replication, but can contribute the virus's pathogenicity (15). One of SARS-CoV-2's accessory proteins, ORF6, was recently shown to co-purify with Rae1 and Nup98 in an affinity purification mass spectrometry screen (13). Similar to VSV M and KSHV ORF10, SARS-CoV-2 ORF6 contains a methionine in its C-terminus that is surrounded by acidic residues, which may facilitate an interaction with the nucleic binding site of the Rae1•Nup98 complex (13). The impact of the putative ORF6-Rae1-Nup98 interactions on export of host mRNA and protein expression has yet to be determined.

In the closely related severe acute respiratory syndrome coronavirus (SARS-CoV), ORF6 was shown to block nuclear import of STAT1 by binding the importin karyopherin alpha 2 (16). SARS-CoV ORF6 has also been shown to downregulate expression of co-transfected constructs (17). However, it is unclear if SARS-CoV ORF6 mediates this repression by restricting mRNA nuclear export via interactions with Rae1 or Nup98.

Results

Identification of a 9 amino acid deletion in ORF6 independently arising in multiple clinical SARS-CoV-2 isolates and a serially passaged cultured isolate

While sequencing clinical SARS-CoV-2 isolates, we identified a unique isolate (WA-UW-4752, MT798143) containing a 27-nucleotide, in-frame deletion within ORF6. The isolate was derived from a nasopharyngeal swab (C_T 26.1, Hologic Panther Fusion) from an individual who presented to the emergency room after 8 days of fever, cough, and myalgias and was on no specific COVID-19 therapy. The resulting ORF6 protein,

96 referred to as ORF6 Δ22-30, contains a 9-amino acid deletion towards the N-terminus of
97 ORF6 (Figure 1A). The deletion was confirmed by RT-PCR and Sanger sequencing
98 (Figure 1B).
99 We searched for similar ORF6 deletions in over 67,000 SARS-CoV-2 genomes
100 present in GISAID (accessed July 17, 2020) and identified 6 other clinical isolates
101 collected in Virginia, California, Belgium, and the United Kingdom that contained the
102 same ORF6 deletion (Table S1). Additionally, we identified a SARS-CoV-2 isolate with
103 an identical deletion that arose after six serial passages in cell culture (Table S1) (18).
104 Notably, the original clinical isolate used to infect the cells had an intact ORF6 (18). We
105 next performed a phylogenetic analysis (Figure 1C) to determine the genetic
106 relatedness of the 8 strains. The strains differed by 2 – 20 single nucleotide variants and
107 belonged to 4 different lineages, A, A.1, B.1, and B.1.5, as defined by Pangolin
108 (https://github.com/cov-lineages/pangolin) (19), suggesting the ORF6 Δ22-30 deletion
109 arose independently in multiple lineages.
110
111 *ORF6 downregulates expression of a co-transfected mCherry reporter*
112 ORF6 putatively interacts with the nuclear export factor Rae1 and the nuclear pore
113 complex component Nup98 (13). VSV M and KSHV ORF10, which both interact with
114 Rae1 and Nup98, downregulate expression of fluorescent or luminescent reporters
115 when co-transfected in cell culture by preventing nuclear export of reporter mRNA (6,
116 8). We generated a series of N-terminal GFP-tagged ORF6 constructs (Figure 2A) and
117 co-transfected 293T cells with these constructs and a reporter plasmid encoding
118 mCherry. Similar to VSV M, cells expressing the GFP-ORF6 construct showed a

119 significant reduction in mCherry expression (Mean Fluorescent Intensity [MFI]: 0.31;
120 Standard Error [SE]: 0.01; p = 0.01) relative to the cells transfected with GFP alone
121 (MFI: 1.0; SE: 0.09) (Figure 2B-C). Subsequent western blotting and densitometry
122 (Figure 2D-E) further confirmed mCherry expression was downregulated in cells
123 expressing wild-type (WT) ORF6.

124 ORF6 constructs containing deletions in the protein's N-terminus, ORF6 Δ1-16
125 (MFI: 0.23, SE: 0.03) and the clinical isolate variant ORF6 Δ22-30 (MFI: 0.31; SE: 0.01),
126 displayed a 3- to 4-fold reduction in mCherry expression (Figure 2B-C) similar to WT
127 ORF6, indicating the N-terminus of ORF6 is not involved in downregulating protein
128 expression. In contrast, mCherry expression was only reduced 1.4- to 1.5-fold in the
129 presence of ORF6 constructs with deletions in the C-terminus, ORF6 Δ38-61 (MFI:
130 0.71; SE: 0.08) and Δ50-61 (MFI: 0.66; SE: 0.03) (Figure 2B-C).

131 In VSV M, a motif consisting of a methionine residue surrounded by acidic
132 residues is critical for reducing expression levels of co-transfected reporters. The
133 methionine residue within the motif is conserved between VSV M and KSHV ORF10
134 and a similar motif with a methionine residue is present in the SARS-CoV-2 ORF6 C-
135 terminus (Figure 1A). We substituted this methionine residue in ORF6 to an alanine,
136 generating the construct ORF6 Met58Ala (Figure 2A). Transfection of ORF6 Met58Ala
137 did not downregulate mCherry expression (MFI: 1.08; SE: 0.09) (Figure 2B-C)
138 suggesting Met58 is critical for the function of ORF6.

139

140 *mRNA accumulates in the nucleus in the presence of ORF6*

We next investigated whether the reduced mCherry expression observed in the presence of ORF6 was due to the impairment of mRNA nuclear export. We transfected cells with either GFP, GFP-tagged WT ORF6, GFP-tagged ORF6 Met58Ala, or GFP-tagged VSV M and stained the cells with an oligo dT(30) fluorescent probe to visualize mRNA distribution within the transfected cells (Figure 3). In cells transfected with GFP or ORF6 Met58Ala, mRNA was distributed throughout the cell indistinguishable from the mRNA localization pattern in un-transfected cells. In contrast, mRNA in cells expressing WT ORF6 and VSV M was present in multiple foci within the nucleus suggesting the mRNA in these cells was accumulating in the nucleus. The mRNA localization patterns are consistent with the reporter expression (Figure 2B-D) indicating that the downregulation in reporter expression is due to impairment of mRNA nuclear export.

The C-terminus of SARS-CoV-2 ORF6 interacts with Rae1 and Nup98

In VSV M and KSHV ORF10, downregulation of co-transfected fluorescent and luminescent reporters and impairment of mRNA nuclear export occurs due to interactions with the nuclear mRNA export factor Rae1 and nuclear pore complex component Nup98 (6, 8). VSV M displaces single stranded RNA in the Rae1•Nup98 complex to prevent nuclear export of host mRNA (11). We hypothesized the inability of the ORF6 C-terminal deletions to downregulate mCherry expression in a similar manner as WT ORF6 (Figure 2B-E) was attributed to the loss of the interaction between these ORF6 constructs and Rae1 and Nup98. We transfected 293T cells with GFP-tagged ORF6 constructs (Figure 2A) and rapidly affinity purified the GFP-tagged proteins. Western blotting on the elutes confirmed WT ORF6, along with ORF6 constructs with N-

terminal deletions, interacts with Rae1 and Nup98 (Figure 4). The C-terminal deletion constructs, ORF6 Δ38-61 and ORF6 Δ50-61, did not pull down Rae1 or Nup98 (Figure 4). These data suggest the C-terminus of ORF6 interacts with Rae1 and Nup98, while the N-terminus is not essential for the observed interactions. This is consistent with the observation that C-terminal deletion mutants of ORF6 did not dramatically reduce expression of the mCherry reporter (Figure 2B-E).

The methionine residue in the Rae1-Nup98 interacting motif of VSV M forms multiple intermolecular interactions with amino acid residues in the nucleic acid binding site of Rae1 and facilitates the interaction between VSV M and the Rae1•Nup98 complex (11). We hypothesized Met58 of SARS-CoV-2 ORF6 is similarly responsible for interactions with Rae1 and Nup98. Affinity purification of ORF6 Met58Ala revealed it does not interact with Rae1 or Nup98 (Figure 4), confirming the importance of Met58 in the ORF6-Rae1 and ORF6-Nup98 interactions.

Overexpression of Rae1 restores mCherry reporter expression in cells transfected with ORF6

We next investigated whether we could restore mCherry expression in 293T cells transfected with ORF6 by overexpressing Rae1. Rae1 overexpression restored mCherry expression in a dose-dependent manner (Figure 5A-B). Subsequent western blotting and densitometry confirmed this Rae1 dose-dependent rescue of mCherry expression (Figure 5C-D). These data indicate ORF6's interaction with Rae1 is responsible for downregulating mCherry reporter expression in cell culture.

187 *SARS-CoV-2 ORF6 more strongly co-purifies with Rae1 and Nup98 compared to*
188 *SARS-CoV ORF6*

189 We next compared the relative ability of SARS-CoV ORF6 and SARS-CoV-2 ORF6 to
190 downregulate reporter expression. SARS-CoV ORF6 and SARS-CoV-2 ORF6 share
191 69% identity by amino acid, including the same methionine residue surrounded by
192 acidic residues (Figure 6A). SARS-CoV ORF6 has been shown to downregulate
193 expression of a co-transfected construct in a dose-dependent manner (19), suggesting
194 its C-terminus may also interact with the Rae1•Nup98 complex.

195 We co-transfected 293T cells with GFP-tagged SARS-CoV ORF6 or GFP-tagged
196 SARS-CoV-2 ORF6 and mCherry to assess the impact of these constructs on protein
197 expression. Compared to cells transfected with GFP alone, cells transfected with SARS-
198 CoV ORF6 displayed reduced mCherry expression (MFI: 1; SE: 0.08 vs. MFI: 0.71, SE:
199 0.03), however this difference was not significant ($p = 0.06$) (Figure 6B-C). Cells
200 transfected with SARS-CoV-2 ORF6 displayed a significant reduction in mCherry
201 expression compared to cells transfected with SARS-CoV ORF6 (MFI: 0.3; SE: 0.02; p
202 $= 0.001$) (Figure 6B-C). Western blotting also demonstrated decreased expression of
203 SARS-CoV-2 ORF6 relative to SARS-CoV ORF6, suggesting expression levels do not
204 explain the differential effects on reporter gene expression (Figure 6D).

205 We hypothesized the differences in mCherry expression between SARS-CoV
206 ORF6 and SARS-CoV-2 ORF6 could be attributed to differences in co-purification of
207 Rae1 and Nup98. We transfected 293T cells with the GFP-tagged constructs and
208 affinity purified the tagged-proteins. Western blotting revealed SARS-CoV ORF6
209 interacts with Rae1 and Nup98 similar to SARS-CoV-2 ORF6 (Figure 6E). Densitometry

on the ratio of prey-to-bait demonstrated SARS-CoV-2 ORF6 co-purified with 1.3-fold more Rae1 (Figure 6F) and 3.8-fold more Nup98 (Figure 6G) compared to SARS-CoV ORF6. These data suggest SARS-CoV-2 ORF6 may more dramatically repress protein expression via a stronger interaction with the Rae1•Nup98 complex compared to SARS-CoV ORF6.

Discussion

Here, we demonstrate SARS-CoV-2 ORF6 downregulates protein expression and entraps mRNA in the nucleus through interactions with the mRNA nuclear export factor Rae1 and the nuclear pore complex component Nup98. We show reporter repression, mRNA nuclear export, and the host-viral protein-protein interactions are critically dependent on a methionine residue in the ORF6 C-terminus. Additionally, we demonstrate an ORF6 allele with a 9-amino acid deletion which has arisen in multiple clinical SARS-CoV-2 isolates and a serially passaged culture isolate maintains the ability to downregulate expression of co-transfected reporter and interact with Rae1 and Nup98. Finally, we found that SARS-CoV-2 ORF6 more strongly represses reporter expression and more strongly copurifies with Rae1-Nup98 compared to SARS-CoV ORF6.

RNA viruses, including coronaviruses, that replicate in the cytoplasm have mechanisms to suppress cellular translation, which allows these viruses use the host's translational machinery to preferentially express viral proteins (1–3). In SARS-CoV, ORF6 is not required for growth *in vitro*, however, expression of SARS-CoV ORF6 can increase the replication kinetics of SARS-CoV and the related murine hepatitis virus *in*

vitro (20, 21). In addition, recombinant SARS-CoV isolates containing ORF6 grow to higher viral loads than recombinant isolates lacking ORF6 (20). This enhancement in viral growth could be attributed to SARS-CoV ORF6's ability to downregulate cellular protein expression through interactions with the Rae1•Nup98 complex. As SARS-CoV-2 ORF6 similarly interacts with Rae1 and Nup98, we speculate ORF6 is required for optimal growth of SARS-CoV-2.

In addition to enhancing viral replication, preventing the nuclear export of mRNA can suppress the host's antiviral response (1–3). The ability of the M protein of VSV to bind Rae1 and Nup98 and prevent mRNA nuclear export is associated with suppressed interferon-ß gene expression (22). Furthermore, VSV strains containing a mutation at the residue responsible for the VSV M-Rae1-Nup98 interactions induce significantly higher interferon-α protein levels than strains containing wild-type alleles of the M protein (23). SARS-CoV-2 ORF6 has been shown to be an interferon antagonist (24) and likely downregulates interferon expression and host antiviral responses in a similar manner to VSV M through its interaction with the Rae1•Nup98 complex.

To date, SARS-CoV-2 has caused several thousand-fold more infections than SARS-CoV in part due to the distinct clinical presentations between the two viruses. COVID-19 patients display peak viral loads and maximum infectivity upon the onset of symptoms rather than after the onset of symptoms which is typical in patient with SARS (25). Furthermore, asymptomatic transmission was infrequently reported for SARS-CoV (26, 27), however, pre-symptomatic and asymptomatic transmission have been a defining challenge of the current SARS-CoV-2 pandemic (28–30). Both the delayed onset of clinical symptoms and pre-symptomatic and asymptomatic transmission of

SARS-CoV-2 could be attributed to increased potency of interferon antagonization in SARS-CoV-2 compared to SARS-CoV. ORF6 has already been shown to be a major interferon antagonist in both SARS-CoV and SARS-CoV-2 (16, 24, 31). ORF6 is one of the least similar accessory proteins (69% identical by amino acid) between the two viruses. Coupled with our demonstration of SARS-CoV-2 ORF6 more strongly downregulating protein expression and co-purifying with more Rae1 and Nup98 than SARS-CoV ORF6, the differences between SARS-CoV ORF6 and SARS-CoV-2 ORF6 could explain at least some of the differences in clinical presentations between SARS and COVID-19.

Large-scale SARS-CoV-2 genomic surveillance projects have demonstrated deletions can arise within the accessory genes of SARS-CoV-2 (32–34). Notably, none of these deletions have arisen in multiple SARS-CoV-2 lineages through multiple independent genomic rearrangement events. Our identification of 7 unrelated clinical isolates with the same ORF6 deletion suggests this deletion may be repeatedly selected for in SARS-CoV-2. This is further evidenced by the identification of a cultured SARS-CoV-2 that acquired the same deletion after successive passages in Vero cells (18). Similar to wild-type ORF6 allele, the clinical allele, ORF6 Δ22-30, can repress expression of a co-transfected reporter and still retains the Rae1•Nup98 interacting motif of ORF6. Further work is required to understand the functional role of the ORF6 N-terminus and determine the selective pressures which are repeatedly selecting for the observed deletion.

Our study has a number of limitations. We relied on cellular overexpression systems of ORF6 which rely on nuclear export, making study of a likely nuclear export

inhibition factor difficult. As such, our results may not perfectly reflect the degree to which host mRNA nuclear export and protein expression is downregulated during SARS-CoV-2 infection, which does not rely on nuclear export for ORF6 expression. More comparative work between SARS-CoV-2 and SARS-CoV ORF6 is needed in the context of viral replication. It would be intriguing to swap ORF6 between SARS-CoV and SARS-CoV-2 isolates to test the hypothesis that ORF6 is the major determinant of interferon antagonization and delayed symptom onset in animal models of SARS-CoV-2. Furthermore, additional work is required to understand the degree of mRNA export inhibition in both viruses.

In summary, our results demonstrate the accessory protein ORF6 of SARS-CoV-2 strongly inhibits reporter protein expression and imprisons mRNA in the nucleus via its interactions with the mRNA nuclear export factor Rae1 and the nuclear pore complex component Nup98. As ORF6 is a major interferon antagonist in *Sarbecoviruses*, differences in ORF6 sequence content may be major determinants of differences in clinical presentation among these viruses that so clearly have the world's attention.

Methods

Specimen collection and whole genome sequencing of SARS-CoV-2 positive clinical specimens

Whole genome sequencing of SARS-CoV-2 positive clinical specimens was conducted as part of an ongoing University of Washington Institutional Review Board-approved study (STUDY00000408) (35–38). Nasopharyngeal swabs were collected from patients suspected to have an infection with SARS-CoV-2 and stored in 3 mL of viral transport

medium. RNA was extracted from 140 µL of medium using the Qiagen Biorobot. Sequencing libraries were prepared as previously described (32). Briefly, RNA was treated with TURBO DNase (Thermo Fisher) and first-strand cDNA was synthesized using Superscript IV (Thermo Fisher) and random hexamers (IDT). Double stranded cDNA was created using Sequenase Version 2.0 (Thermo Fisher) and purified using 1.6x volumes of AMPure XP beads (Beckman-Coulter). Multiplex amplicon sequencing libraries were constructed using Swift Biosciences' SARS-CoV-2 Multiplex Primer Pool and Normalase Amplicon kit and sequenced on a 2 x 300 bp run on an Illumina MiSeq.

712,394 sequencing reads were obtained for the clinical SARS-CoV-2 sample, WA-UW-4752. Sequencing reads were quality- and adapter-trimmed using Trimmomatic v0.38 (ILLUMINACLIP:TruSeq3-PE-SNAP.fa:2:30:10:1:true LEADING:3 TRAILING:3 SLIDINGWINDOW:4:30 MINLEN:75) (39) and aligned to the SARS-CoV-2 reference genome (NC_045512.2) using BBMap version 38.70 (sourceforge.net/projects/bbmap/). Sequence reads were then clipped of synthetic PCR primers using Primerclip (https://github.com/swiftbiosciences/primerclip) and the final sequence alignment was visualized in Geneious version 11.1.4 (40).

The deletion identified within ORF6 of WA-UW-4752 was confirmed by reverse transcription PCR and Sanger sequencing. For reverse transcription, single-stranded cDNA was constructed using Superscript IV. The resulting cDNA was used as template for PCR with Phusion High-Fidelity Polymerase (Thermo Fisher) and the following primers: 5' ATCACGAACGCTTTCTTATTAC 3' and 5' CTCGTATGTTCCAGAAGAGC 3'. PCR was conducted using the following conditions: 98ºC for 30 seconds followed by 35 cycles of 98ºC for 10 seconds, 55ºC for 15 seconds, and 72ºC for 30 seconds

325 followed by a final extension at 72ºC for 5 minutes. The resulting amplicons were run on
326 a 2% agarose gel, extracted from the gel using the QIAquick Gel Extraction kit (Qiagen),
327 and Sanger sequenced by Genewiz, Inc. with the same primers used for PCR.
328 Other strains with the same deletion in ORF6 were identified by querying GISAID
329 (accessed July 17, 2020). The genetic relatedness of these strains was assessed by
330 aligning the genomes of these strains as well as 110 other global clinical SAR-CoV-2
331 strains using MAFFT v7.453 (41). A phylogenetic tree was generated using RAxML
332 version 8.2.11 (42) and visualized with R (version 3.6.1) using the ggtree package (43).
333 Strains were further classified using the web-based lineage assigner, Pangolin
334 (https://pangolin.cog-uk.io/) (19).
335
336 *Cloning*
337 The wild-type, N- and C-terminal mutant SARS-CoV-2 ORF6 constructs were amplified
338 from double-stranded cDNA from a previously sequenced clinical SARS-CoV-2 isolate
339 (WA12-UW8; EPI_ISL_413563) using the primers listed in Table S2. CloneAmp Hi-Fi
340 PCR Premix (Takara) and the following PCR conditions were used to generate the
341 amplicons: 98ºC for 2 minutes followed by 35 cycles of 98ºC for 10 seconds, 55ºC for
342 15 seconds, and 72ºC for 30 seconds followed by a final extension for 72ºC for 5
343 minutes. ORF6 Δ22-30 was amplified from WA-UW-4572 (MT798143) and the matrix
344 protein from vesicular stomatitis virus was amplified from pVSV eGFP dG (a gift from
345 Connie Cepko; Addgene plasmid #31842) as described above using the primers listed
346 in Table S2. A gBlock gene fragment (IDT) for ORF6 of SARS-CoV was synthesized
347 based on the genome sequence of SARS-CoV isolate TW1 (AY291451.1). The

resulting amplicons and gene fragment were then cloned into a modified pLenti CMV GFP Puro plasmid (a gift from Eric Campeau & Paul Kaufman; Addgene plasmid #17448), which contains a 3' WPRE sequence following the insert and a 3' SV40 polyadenylation signal after the puromycin resistance cassette, with an N-terminal GFP tag using the In-Fusion HD Cloning kit (Takara).

For cloning of Rae1, RNA was extracted from 239T cells using the RNeasy Miniprep kit (Qiagen) and cDNA was synthesized using Superscript IV and oligo dT (IDT). Rae1 was then amplified from the resulting cDNA using the primers listed in Table S2 and CloneAmp Hi-Fi PCR Premix under the following PCR conditions: 98ºC for 2 minutes followed by 35 cycles of 98ºC for 10 seconds, 55ºC for 15 seconds, and 72ºC for 1 minute followed by a final extension for 72ºC for 5 minutes. The resulting amplicon was cloned into a modified pcDNA4-TO vector with a C-terminal FLAG tag using the In-Fusion HD Cloning kit.

Cell culture and ORF6-mCherry transient co-transfections

293T cells were maintained in Dulbecco's Modified Eagle's Medium (GE Healthcare Life Sciences) supplemented with 10% FBS (Sigma-Aldrich), 1x HEPES (Thermo Fisher), and 1x GlutaMAX (Thermo Fisher) (293T media). Transient co-transfections with GFP-tagged constructs and a modified pLenti CMV Puro vector encoding the fluorescent reporter mCherry were conducted in 6-well plates. The day prior to transfection, 500,000 293T cells were plated into each well of the 6-well plate and grown overnight until they reached approximately 50% confluency. The cells were then transfected with 2 µg of GFP-tagged construct and 2 µg of mCherry using a 3:1 ratio of PEI MAX

(Polysciences) in Opti-MEM (Thermo Fisher). Cells were incubated for 24-48 hours following transfection and visualized using the EVOS M5000 Imaging System (Thermo Fisher) with GFP and Texas Red filter cubes.

mCherry fluorescence intensities were measured with ImageJ v1.53a by an individual blinded to experimental design. All images were 8-bit grayscale and 2048x1536 (3.1 megapixels). Background thresholds were set at the same level across all images, and mean fluorescence intensity of regions of interest greater than 200 pixels calculated. Three fields were analyzed for each experimental condition. The mean fluorescent intensity for each field was calculated after adjusting for background fluorescence signal and normalized to the control condition. Difference in mean fluorescent intensities between experimental conditions were assessed in R using the unpaired t-test.

Cell lysates were collected 24-48 hours after transfection using RIPA buffer (Thermo Fisher). The total protein content was measured using the Pierce BCA Protein Assay kit (Thermo Fisher) and 7.5 µg of lysate was run on a 4-12% Bis-Tris sodium dodecyl sulfate (SDS)-polyacrylamide gel with MOPS running buffer (Invitrogen) under reducing conditions. The samples were then transferred to a 0.45 µm nitrocellulose membrane using the XCell Blot II module (Invitrogen). Blotting was performed using the following primary antibodies: 1:1,000 anti-GFP (Cell Signaling; clone 4B10), 1:500 anti-mCherry (Cell Signaling; clone E5D8F), and 1:1,000 anti-alpha Tubulin (Cell Signaling; clone DM1A), which was followed by staining with either 1:10,000 IRDye 680RD anti-Mouse IgG secondary antibody (Licor) or 1:5,000 IRDye 800CW anti-Rabbit IgG

393 secondary antibody (Licor). Blots were then visualized on a Licor Odyssey imager using
394 Image Studio version 2.0.
395
396 *Oligo dT in situ hybridization*
397 293T cells were plated in 48-well plates at a density of 60,000 cells per well and grown
398 overnight to approximately 50% confluency. Cells were transfected with 200 ng of
399 plasmid DNA as described above and incubated for 24 hours. The cells were then
400 washed with PBS (pH 7.4; without Ca^{2+} or Mg^{2+}) (Thermo Fisher) and fixed with 4%
401 paraformaldehyde. The fixed cells were permeabilized with methanol and rehydrated in
402 70% ethanol followed by 1M Tris-HCl (pH 8.0) (Invitrogen). The monolayer was then
403 covered with hybridization buffer (1 mg/mL yeast tRNA, 0.005% bovine serum, 10%
404 dextran sulfate and 25% formamide in 2x SSC buffer) containing an oligo dT(30) probe
405 with an Alexa Fluor 594 fluorophore (IDT) attached to the 5' end of the probe and
406 incubate overnight at 37ºC. The hybridization buffer was removed and the cells were
407 washed once with warmed 4x SSC buffer (Thermo Fisher), once with warmed 2x SSC
408 buffer, and twice with room temperature 2x SSC buffer.
409 The cells were then blocked with 1% bovine serum in PBS containing 0.1%
410 Tween 20 (PBST) for 1 hour. To detect the GFP-tagged proteins, the cells were
411 incubated with a FITC conjugated anti-GFP antibody (Abcam) for 1 hour. The antibody
412 was removed and the cells were washed three times with PBST. Nuclear staining was
413 completed by incubating the cells in a 300 nM DAPI solution (Thermo Fisher) for 5
414 minutes. The cells were washed twice with PBS and visualized on an EVOS M5000 with
415 the GFP, Texas Red, and DAPI filter cubes.

Affinity Purification of GFP-tagged constructs

The day prior to transient transfection, 10-cm plates were seeded with $4x10^6$ 293T cells and grown overnight to approximately 50% confluency. The cells were transfected with 7 µg of plasmid DNA using a 3:1 ratio of PEI MAX in Opti-MEM. Forty-four to 48 hours after transfection, the cells were washed with PBS and collected using PBS containing 0.1 mM EDTA. The cells were pelleted, resuspended in 500 µL TEN (50mM Tris 8.0, 150mM NaCl, and 1mM EDTA) buffer with 0.5% NP-40, and lysed by rotation for 45-60 minutes at 4ºC. The lysates were centrifuged at 13,000 RPM for 5 minutes at 4ºC and the supernatant was transferred to a new tube and cleared of residual IgG by rotation with Protein G Sepharose 4 Fast Flow (GE Healthcare Life Sciences) for 30 minutes at 4ºC. Cleared lysates were transferred to new tubes and incubated overnight at 4ºC with anti-GFP Nanobody Affinity gel (BioLegend). The affinity gel was then pelleted and washed twice using TEN buffer with 0.1% NP-40 and resuspended in equal volumes of NuPage LDS Sample Buffer (Thermo) containing 143 mM 2-Mercaptoethanol (Sigma-Aldrich). Western blotting using the elutes from affinity purification and the pre-purified input lysates were performed as described above with the following primary antibodies: 1:1,000 anti-GFP, 1:1,000 anti-alpha Tubulin, 1:2,000 anti-Rae1 (Abcam; clone EPR6923) and 1:1,000 anti-Nup98 (Abcam; clone 2H10).

Rae1 rescue of mCherry expression

293T cells were plated in 6-well plates at a seeding density of 500,000 cells per well and grown overnight until they reached approximately 50% confluency. Cells were then

transfected with 0.5 µg of the GFP-SARS-CoV-2 wild-type ORF6 construct, 0.5 µg of mCherry, and 0, 0.25, 0.5, 1, or 2 µg of Rae1-FLAG using a 3:1 ratio of PEI MAX in Opti-MEM. GFP and mCherry expression were visualized 44-48 hours following transfection using the EVOS M5000 imaging system with GFP and Texas Red filter cubes. Western blotting was performed as described above with the following primary antibodies: 1:1,000 anti-GFP, 1:500 anti-mCherry, 1:1,000 anti-alpha Tubulin, and 1:1,000 anti-FLAG (Sigma; clone M2).

Data Availability

Sequencing reads and genome assemblies are available under NCBI BioProject PRJNA610428.

References

1. Stern-Ginossar N, Thompson SR, Mathews MB, Mohr I. 2019. Translational Control in Virus-Infected Cells. Cold Spring Harb Perspect Biol 11:a033001.

2. Gale M, Tan S-L, Katze MG. 2000. Translational Control of Viral Gene Expression in Eukaryotes. Microbiol Mol Biol Rev 64:239–280.

3. Walsh D, Mohr I. 2011. Viral subversion of the host protein synthesis machinery. Nat Rev Microbiol 9:860–875.

4. Kuss SK, Mata MA, Zhang L, Fontoura BMA. 2013. Nuclear imprisonment: viral strategies to arrest host mRNA nuclear export. Viruses 5:1824–1849.

5. Sandri-Goldin RM. 2004. Viral Regulation of mRNA Export. JVI 78:4389–4396.

6. Faria PA, Chakraborty P, Levay A, Barber GN, Ezelle HJ, Enninga J, Arana C, van Deursen J, Fontoura BMA. 2005. VSV Disrupts the Rae1/mrnp41 mRNA Nuclear Export Pathway. Molecular Cell 17:93–102.

7. Park N, Katikaneni P, Skern T, Gustin KE. 2008. Differential Targeting of Nuclear Pore Complex Proteins in Poliovirus-Infected Cells. JVI 82:1647–1655.

8. Gong D, Kim YH, Xiao Y, Du Y, Xie Y, Lee KK, Feng J, Farhat N, Zhao D, Shu S, Dai X, Chanda SK, Rana TM, Krogan NJ, Sun R, Wu T-T. 2016. A Herpesvirus Protein Selectively Inhibits Cellular mRNA Nuclear Export. Cell Host Microbe 20:642–653.

9. Pritchard CE, Fornerod M, Kasper LH, van Deursen JM. 1999. RAE1 is a shuttling mRNA export factor that binds to a GLEBS-like NUP98 motif at the nuclear pore complex through multiple domains. J Cell Biol 145:237–254.

10. Ren Y, Seo H-S, Blobel G, Hoelz A. 2010. Structural and functional analysis of the interaction between the nucleoporin Nup98 and the mRNA export factor Rae1. Proceedings of the National Academy of Sciences 107:10406–10411.

11. Quan B, Seo H-S, Blobel G, Ren Y. 2014. Vesiculoviral matrix (M) protein occupies nucleic acid binding site at nucleoporin pair (Rae1 • Nup98). Proc Natl Acad Sci USA 111:9127–9132.

12. Rajani KR, Pettit Kneller EL, McKenzie MO, Horita DA, Chou JW, Lyles DS. 2012. Complexes of Vesicular Stomatitis Virus Matrix Protein with Host Rae1 and Nup98 Involved in Inhibition of Host Transcription. PLoS Pathog 8:e1002929.

13. Gordon DE, Jang GM, Bouhaddou M, Xu J, Obernier K, White KM, O'Meara MJ, Rezelj VV, Guo JZ, Swaney DL, Tummino TA, Huettenhain R, Kaake RM, Richards AL, Tutuncuoglu B, Foussard H, Batra J, Haas K, Modak M, Kim M, Haas P, Polacco BJ, Braberg H, Fabius JM, Eckhardt M, Soucheray M, Bennett MJ, Cakir M, McGregor MJ, Li Q, Meyer B, Roesch F, Vallet T, Mac Kain A, Miorin L, Moreno E, Naing ZZC, Zhou Y, Peng S, Shi Y, Zhang Z, Shen W, Kirby IT, Melnyk JE, Chorba JS, Lou K, Dai SA, Barrio-Hernandez I, Memon D, Hernandez-Armenta C, Lyu J, Mathy CJP, Perica T, Pilla KB, Ganesan SJ, Saltzberg DJ, Rakesh R, Liu X, Rosenthal SB, Calviello L, Venkataramanan S, Liboy-Lugo J, Lin Y, Huang X-P, Liu Y, Wankowicz SA, Bohn M, Safari M, Ugur FS, Koh C, Savar NS, Tran QD,

Shengjuler D, Fletcher SJ, O'Neal MC, Cai Y, Chang JCJ, Broadhurst DJ, Klippsten S, Sharp PP, Wenzell NA, Kuzuoglu D, Wang H-Y, Trenker R, Young JM, Cavero DA, Hiatt J, Roth TL, Rathore U, Subramanian A, Noack J, Hubert M, Stroud RM, Frankel AD, Rosenberg OS, Verba KA, Agard DA, Ott M, Emerman M, Jura N, von Zastrow M, Verdin E, Ashworth A, Schwartz O, d'Enfert C, Mukherjee S, Jacobson M, Malik HS, Fujimori DG, Ideker T, Craik CS, Floor SN, Fraser JS, Gross JD, Sali A, Roth BL, Ruggero D, Taunton J, Kortemme T, Beltrao P, Vignuzzi M, García-Sastre A, Shokat KM, Shoichet BK, Krogan NJ. 2020. A SARS-CoV-2 protein interaction map reveals targets for drug repurposing. Nature https://doi.org/10.1038/s41586-020-2286-9.

14. Zhu N, Zhang D, Wang W, Li X, Yang B, Song J, Zhao X, Huang B, Shi W, Lu R, Niu P, Zhan F, Ma X, Wang D, Xu W, Wu G, Gao GF, Tan W. 2020. A Novel Coronavirus from Patients with Pneumonia in China, 2019. N Engl J Med 382:727–733.

15. Narayanan K, Huang C, Makino S. 2008. SARS coronavirus accessory proteins. Virus Research 133:113–121.

16. Frieman M, Yount B, Heise M, Kopecky-Bromberg SA, Palese P, Baric RS. 2007. Severe acute respiratory syndrome coronavirus ORF6 antagonizes STAT1 function by sequestering nuclear import factors on the rough endoplasmic reticulum/Golgi membrane. J Virol 81:9812–9824.

17. Gunalan V, Mirazimi A, Tan Y-J. 2011. A putative diacidic motif in the SARS-CoV ORF6 protein influences its subcellular localization and suppression of expression of co-transfected expression constructs. BMC Res Notes 4:446.

18. Riojas MA, Frank AM, Puthuveetil NP, Flores B, Parker M, King SP, Peiris M, Chu DKW, Benton B, Bradford R, Hazbón MH, Rashid S. 2020. A Rare Deletion in SARS-CoV-2 ORF6 Dramatically Alters the Predicted Three-Dimensional Structure of the Resultant Protein. preprint, Genomics.

19. Rambaut A, Holmes EC, Hill V, O'Toole Á, McCrone J, Ruis C, du Plessis L, Pybus OG. 2020. A dynamic nomenclature proposal for SARS-CoV-2 to assist genomic epidemiology. preprint, Microbiology.

20. Zhao J, Falcón A, Zhou H, Netland J, Enjuanes L, Pérez Breña P, Perlman S. 2009. Severe Acute Respiratory Syndrome Coronavirus Protein 6 Is Required for Optimal Replication. JVI 83:2368–2373.

21. Hussain S, Perlman S, Gallagher TM. 2008. Severe Acute Respiratory Syndrome Coronavirus Protein 6 Accelerates Murine Hepatitis Virus Infections by More than One Mechanism. JVI 82:7212–7222.

22. Ahmed M, McKenzie MO, Puckett S, Hojnacki M, Poliquin L, Lyles DS. 2003. Ability of the Matrix Protein of Vesicular Stomatitis Virus To Suppress Beta Interferon Gene Expression Is Genetically Correlated with the Inhibition of Host RNA and Protein Synthesis. JVI 77:4646–4657.

532 23. Stojdl DF, Lichty BD, tenOever BR, Paterson JM, Power AT, Knowles S, Marius R,
533 Reynard J, Poliquin L, Atkins H, Brown EG, Durbin RK, Durbin JE, Hiscott J, Bell
534 JC. 2003. VSV strains with defects in their ability to shutdown innate immunity are
535 potent systemic anti-cancer agents. Cancer Cell 4:263–275.

536 24. Yuen C-K, Lam J-Y, Wong W-M, Mak L-F, Wang X, Chu H, Cai J-P, Jin D-Y, To
537 KK-W, Chan JF-W, Yuen K-Y, Kok K-H. 2020. SARS-CoV-2 nsp13, nsp14, nsp15
538 and orf6 function as potent interferon antagonists. Emerging Microbes & Infections
539 9:1418–1428.

540 25. Petersen E, Koopmans M, Go U, Hamer DH, Petrosillo N, Castelli F, Storgaard M,
541 Al Khalili S, Simonsen L. 2020. Comparing SARS-CoV-2 with SARS-CoV and
542 influenza pandemics. The Lancet Infectious Diseases S1473309920304849.

543 26. Wilder-Smith A, Teleman MD, Heng BH, Earnest A, Ling AE, Leo YS. 2005.
544 Asymptomatic SARS Coronavirus Infection among Healthcare Workers, Singapore.
545 Emerg Infect Dis 11:1142–1145.

546 27. Lee HKK, Tso EYK, Chau TN, Tsang OTY, K, Choi W, Lai TST. 2003.
547 Asymptomatic Severe Acute Respiratory Syndrome–associated Coronavirus
548 Infection. Emerg Infect Dis 9:1491–1492.

549 28. Bai Y, Yao L, Wei T, Tian F, Jin D-Y, Chen L, Wang M. 2020. Presumed
550 Asymptomatic Carrier Transmission of COVID-19. JAMA 323:1406.

551 29. Wei WE, Li Z, Chiew CJ, Yong SE, Toh MP, Lee VJ. 2020. Presymptomatic
552 Transmission of SARS-CoV-2 - Singapore, January 23-March 16, 2020. MMWR
553 Morb Mortal Wkly Rep 69:411–415.

554 30. Roxby AC, Greninger AL, Hatfield KM, Lynch JB, Dellit TH, James A, Taylor J,
555 Page LC, Kimball A, Arons M, Schieve LA, Munanga A, Stone N, Jernigan JA,
556 Reddy SC, Lewis J, Cohen SA, Jerome KR, Duchin JS, Neme S. 2020. Detection
557 of SARS-CoV-2 Among Residents and Staff Members of an Independent and
558 Assisted Living Community for Older Adults - Seattle, Washington, 2020. MMWR
559 Morb Mortal Wkly Rep 69:416–418.

560 31. Kopecky-Bromberg SA, Martínez-Sobrido L, Frieman M, Baric RA, Palese P. 2007.
561 Severe acute respiratory syndrome coronavirus open reading frame (ORF) 3b,
562 ORF 6, and nucleocapsid proteins function as interferon antagonists. J Virol
563 81:548–557.

564 32. Addetia A, Xie H, Roychoudhury P, Shrestha L, Loprieno M, Huang M-L, Jerome
565 KR, Greninger AL. 2020. Identification of multiple large deletions in ORF7a
566 resulting in in-frame gene fusions in clinical SARS-CoV-2 isolates. Journal of
567 Clinical Virology 129:104523.

568 33. Holland LA, Kaelin EA, Maqsood R, Estifanos B, Wu LI, Varsani A, Halden RU,
569 Hogue BG, Scotch M, Lim ES. 2020. An 81 nucleotide deletion in SARS-CoV-2
570 ORF7a identified from sentinel surveillance in Arizona (Jan-Mar 2020). J Virol
571 JVI.00711-20, jvi;JVI.00711-20v1.

572 34. Su YC, Anderson DE, Young BE, Zhu F, Linster M, Kalimuddin S, Low JG, Yan Z,
573 Jayakumar J, Sun L, Yan GZ, Mendenhall IH, Leo Y-S, Lye DC, Wang L-F, Smith
574 GJ. 2020. Discovery of a 382-nt deletion during the early evolution of SARS-CoV-2.
575 preprint, Microbiology.

576 35. Fauver JR, Petrone ME, Hodcroft EB, Shioda K, Ehrlich HY, Watts AG, Vogels
577 CBF, Brito AF, Alpert T, Muyombwe A, Razeq J, Downing R, Cheemarla NR, Wyllie
578 AL, Kalinich CC, Ott IM, Quick J, Loman NJ, Neugebauer KM, Greninger AL,
579 Jerome KR, Roychoudhury P, Xie H, Shrestha L, Huang M-L, Pitzer VE, Iwasaki A,
580 Omer SB, Khan K, Bogoch II, Martinello RA, Foxman EF, Landry ML, Neher RA,
581 Ko AI, Grubaugh ND. 2020. Coast-to-Coast Spread of SARS-CoV-2 during the
582 Early Epidemic in the United States. Cell 181:990-996.e5.

583 36. Bedford T, Greninger AL, Roychoudhury P, Starita LM, Famulare M, Huang M-L,
584 Nalla A, Pepper G, Reinhardt A, Xie H, Shrestha L, Nguyen TN, Adler A,
585 Brandstetter E, Cho S, Giroux D, Han PD, Fay K, Frazar CD, Ilcisin M, Lacombe K,
586 Lee J, Kiavand A, Richardson M, Sibley TR, Truong M, Wolf CR, Nickerson DA,
587 Rieder MJ, Englund JA, the Seattle Flu Study Investigators, Hadfield J, Hodcroft
588 EB, Huddleston J, Moncla LH, Müller NF, Neher RA, Deng X, Gu W, Federman S,
589 Chiu C, Duchin J, Gautom R, Melly G, Hiatt B, Dykema P, Lindquist S, Queen K,
590 Tao Y, Uehara A, Tong S, MacCannell D, Armstrong GL, Baird GS, Chu HY,
591 Shendure J, Jerome KR. 2020. Cryptic transmission of SARS-CoV-2 in
592 Washington State. preprint, Epidemiology.

593 37. Deng X, Gu W, Federman S, du Plessis L, Pybus OG, Faria NR, Wang C, Yu G,
594 Bushnell B, Pan C-Y, Guevara H, Sotomayor-Gonzalez A, Zorn K, Gopez A,
595 Servellita V, Hsu E, Miller S, Bedford T, Greninger AL, Roychoudhury P, Starita
596 LM, Famulare M, Chu HY, Shendure J, Jerome KR, Anderson C, Gangavarapu K,
597 Zeller M, Spencer E, Andersen KG, MacCannell D, Paden CR, Li Y, Zhang J, Tong
598 S, Armstrong G, Morrow S, Willis M, Matyas BT, Mase S, Kasirye O, Park M,
599 Masinde G, Chan C, Yu AT, Chai SJ, Villarino E, Bonin B, Wadford DA, Chiu CY.
600 2020. Genomic surveillance reveals multiple introductions of SARS-CoV-2 into
601 Northern California. Science 369:582–587.

602 38. Lieberman NAP, Peddu V, Xie H, Shrestha L, Huang M-L, Mears MC, Cajimat MN,
603 Bente DA, Shi P-Y, Bovier F, Roychoudhury P, Jerome KR, Moscona A, Porotto M,
604 Greninger AL. 2020. *In vivo* antiviral host response to SARS-CoV-2 by viral load,
605 sex, and age. preprint, Microbiology.

606 39. Bolger AM, Lohse M, Usadel B. 2014. Trimmomatic: a flexible trimmer for Illumina
607 sequence data. Bioinformatics 30:2114–2120.

608 40. Kearse M, Moir R, Wilson A, Stones-Havas S, Cheung M, Sturrock S, Buxton S,
609 Cooper A, Markowitz S, Duran C, Thierer T, Ashton B, Meintjes P, Drummond A.
610 2012. Geneious Basic: An integrated and extendable desktop software platform for
611 the organization and analysis of sequence data. Bioinformatics 28:1647–1649.

612 41. Katoh K, Standley DM. 2013. MAFFT multiple sequence alignment software
613 version 7: improvements in performance and usability. Mol Biol Evol 30:772–780.

614 42. Stamatakis A. 2014. RAxML version 8: a tool for phylogenetic analysis and post-
615 analysis of large phylogenies. Bioinformatics 30:1312–1313.

616 43. Yu G, Smith DK, Zhu H, Guan Y, Lam TT-Y. 2017. GGTREE□: an R package for
617 visualization and annotation of phylogenetic trees with their covariates and other
618 associated data. Methods Ecol Evol 8:28–36.

619

620

621 **Figure Legends**

622 **Figure 1.** Multiple clinical SARS-CoV-2 isolates and a serially passaged cultured SARS-
623 CoV-2 isolate contain a 9-amino acid deletion in ORF6. A) Schematic representation of
624 the 9-amino acid deletion in ORF6 identified through whole genome sequencing of the
625 clinical SARS-CoV-2 clinical isolate, WA-UW-4572. B) RT-PCR with primers spanning
626 ORF6 yielded a 452 bp PCR product for WA-UW-4572 rather than a 479 bp product
627 confirming the ORF6 deletion in WA-UW-4572. C) Six other clinical isolates and a
628 cultured isolate with an identified deletion in ORF6 were identified by analyzing the
629 ORF6 sequences of 67,000 publicly available SARS-CoV-2 genomes. The isolates
630 were genetically distinct and belonged to both major SARS-CoV-2 lineages.
631
632 **Figure 2.** ORF6 of SARS-CoV-2 results in reduced mCherry reporter protein expression
633 in 293T cells. A) Schematic representation of ORF6 constructs used in this study. B)
634 293T cells were transiently transfected with GFP-tagged constructs and mCherry and
635 visualized 48 hours after transfection. All images were taken with identical fluorescence
636 gain settings. C) The fluorescent intensities for 3 fields per co-transfection were
637 measured with ImageJ and displayed as mean ± standard error. Wild-type (WT) ORF6
638 caused a significant reduction in mCherry expression. ORF6 constructs with deletions
639 or a single amino acid substitution (Met58Ala) in the C-terminus showed a smaller
640 reduction in mCherry expression than WT ORF6. Cell lysates were collected for each of
641 the conditions and D) western blotting and E) densitometry confirmed the role of the C-
642 terminus of ORF6 in reducing protein expression in transfected cells. * $p < 0.05$; ** $p <$
643 0.01.

644

645 **Figure 3.** ORF6 causes mRNA to accumulate within the nucleus. 293T cells were
646 transiently transfected with GFP-tagged constructs, incubated for 24 hours, and stained
647 for GFP, poly-A mRNA, and DNA. mRNA in cells transfected with GFP or ORF6
648 Met58Ala was diffusely present throughout the cell. Cells transfected with ORF6 or VSV
649 M showed an accumulation of mRNA within the nucleus (white arrows).

650

651 **Figure 4.** Affinity purification of GFP-tagged constructs. 293T were transiently
652 transfected with GFP-tagged constructs. Forty-eight hours after transfection, the GFP-
653 tagged proteins were rapidly captured using an anti-GFP resin. Western blotting
654 revealed ORF6 interacts with the mRNA nuclear export factor Rae1 and the nuclear
655 pore complex protein Nup98. ORF6 constructs with C-terminal deletions or a
656 substitution did not pull down Rae1 or Nup98.

657

658 **Figure 5.** Overexpression of Rae1 rescues mCherry expression in cells transfected with
659 ORF6. A) 293T cells were co-transfected with equal amounts GFP-ORF6 and mCherry
660 and an increasing amount of Rae1. Expression of the fluorescent reporters was
661 visualized and B) quantified 48 hours after transfection. In the presence of ORF6,
662 mCherry expression was restored in a dose-dependent manner. C) Western blotting
663 and D) densitometry confirmed mCherry expression was rescued in a dose-dependent
664 manner with of increasing Rae1-FLAG. * $p < 0.05$.

665

Figure 6. SARS-CoV-2 ORF6 represses reporter expression and copurifies with relatively more Rae1-Nup98 than SARS-CoV ORF6. A) Comparison between the amino acid sequences of ORF6 of SARS-CoV and ORF6 of SARS-CoV-2. Residues differing between the two viruses are highlighted in red. The residue (Met58) implicated in binding the Rae1•Nup98 complex is highlighted in blue. B) 293T were transiently transfected with GFP-tagged constructs and mCherry and visualized 24 hours after transfection. Cells transfected with SARS-CoV-2 ORF6 showed C) significantly reduced mCherry expression compared to those transfected with SARS-CoV ORF6. D) Western blotting showed decreased expression of SARS-CoV-2 ORF6 compared to SARS-CoV ORF6 in 293T cells. E) Affinity purification of GFP-tagged constructs demonstrates both ORF6 of SARS-CoV and ORF6 of SARS-CoV-2 interact with Rae1 and Nup98. Densitometry shows SARS-CoV-2 ORF6 copurifies with relatively more F) Rae1 and G) Nup98 compared SARS-CoV ORF6. * $p < 0.05$; ** $p < 0.01$.

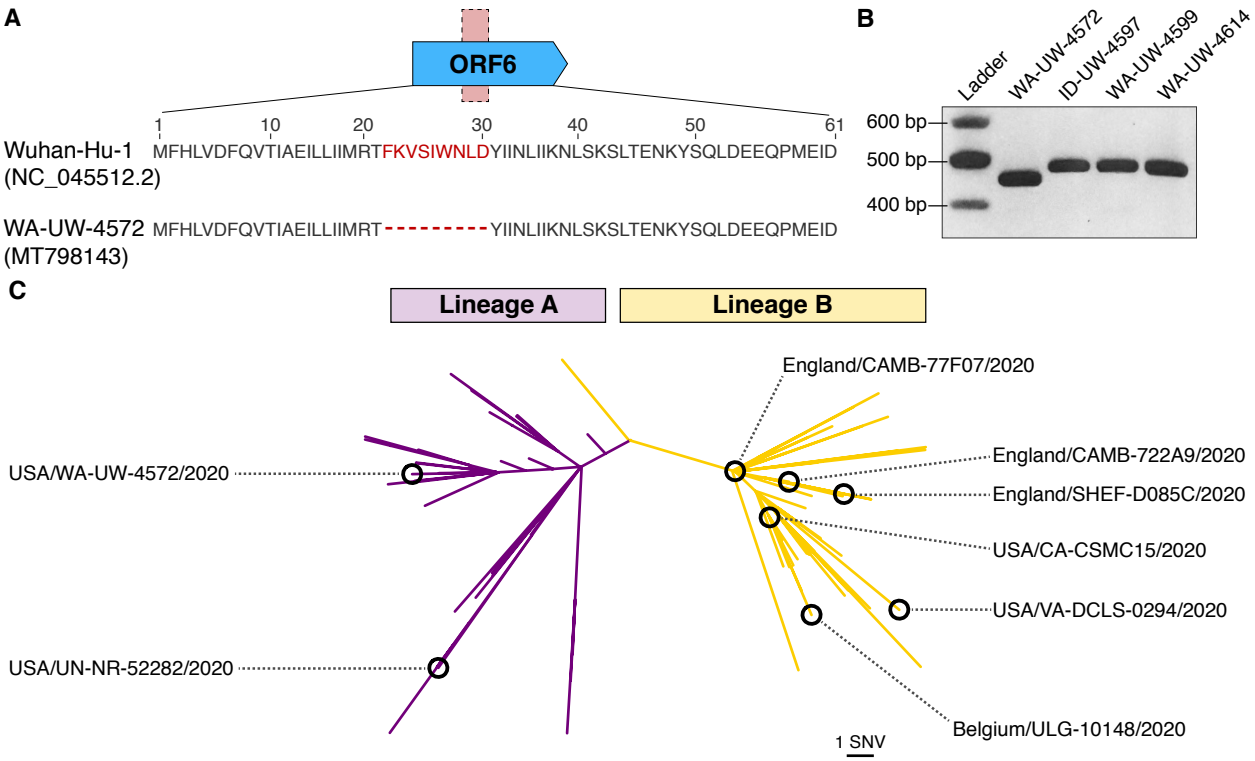

Figure 1. Multiple clinical SARS-CoV-2 isolates and a serially passaged cultured SARS-CoV-2 isolate contain a 9-amino acid deletion in ORF6. A) Schematic representation of the 9-amino acid deletion in ORF6 identified through whole genome sequencing of the clinical SARS-CoV-2 clinical isolate, WA-UW-4572. B) RT-PCR with primers spanning ORF6 yielded a 452 bp PCR product for WA-UW-4572 rather than a 479 bp product confirming the ORF6 deletion in WA-UW-4572. C) Six other clinical isolates and a cultured isolate with an identified deletion in ORF6 were identified by analyzing the ORF6 sequences of 67,000 publicly available SARS-CoV-2 genomes. The isolates were genetically distinct and belonged to both major SARS-CoV-2 lineages.

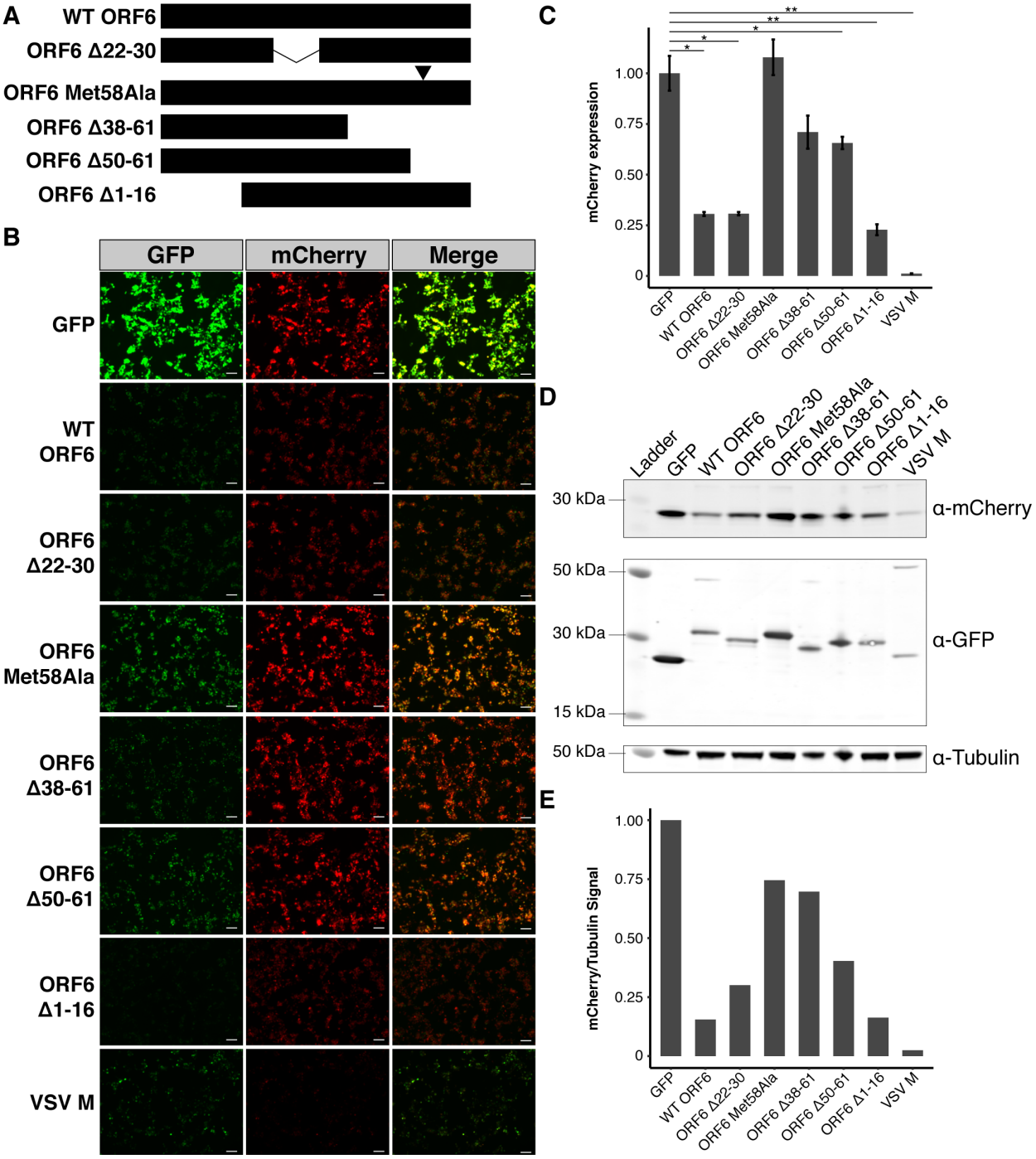

Figure 2. ORF6 of SARS-CoV-2 results in reduced mCherry reporter protein expression in 293T cells. A) Schematic representation of ORF6 constructs used in this study. B) 293T cells were transiently transfected with GFP-tagged constructs and mCherry and visualized 48 hours after transfection. All images were taken with identical fluorescence gain settings. C) The fluorescent intensities for 3 fields per co-transfection were measured with ImageJ and displayed as mean ± standard error. Wild-type (WT) ORF6 caused a significant reduction in mCherry expression. ORF6 constructs with deletions or a single amino acid substitution (Met58Ala) in the C-terminus showed a smaller reduction in mCherry expression than WT ORF6. Cell lysates were collected for each of the conditions and D) western blotting and E) densitometry confirmed the role of the C-terminus of ORF6 in reducing protein expression in transfected cells. * $p < 0.05$; ** $p < 0.01$. Scale bar: 100 μm.

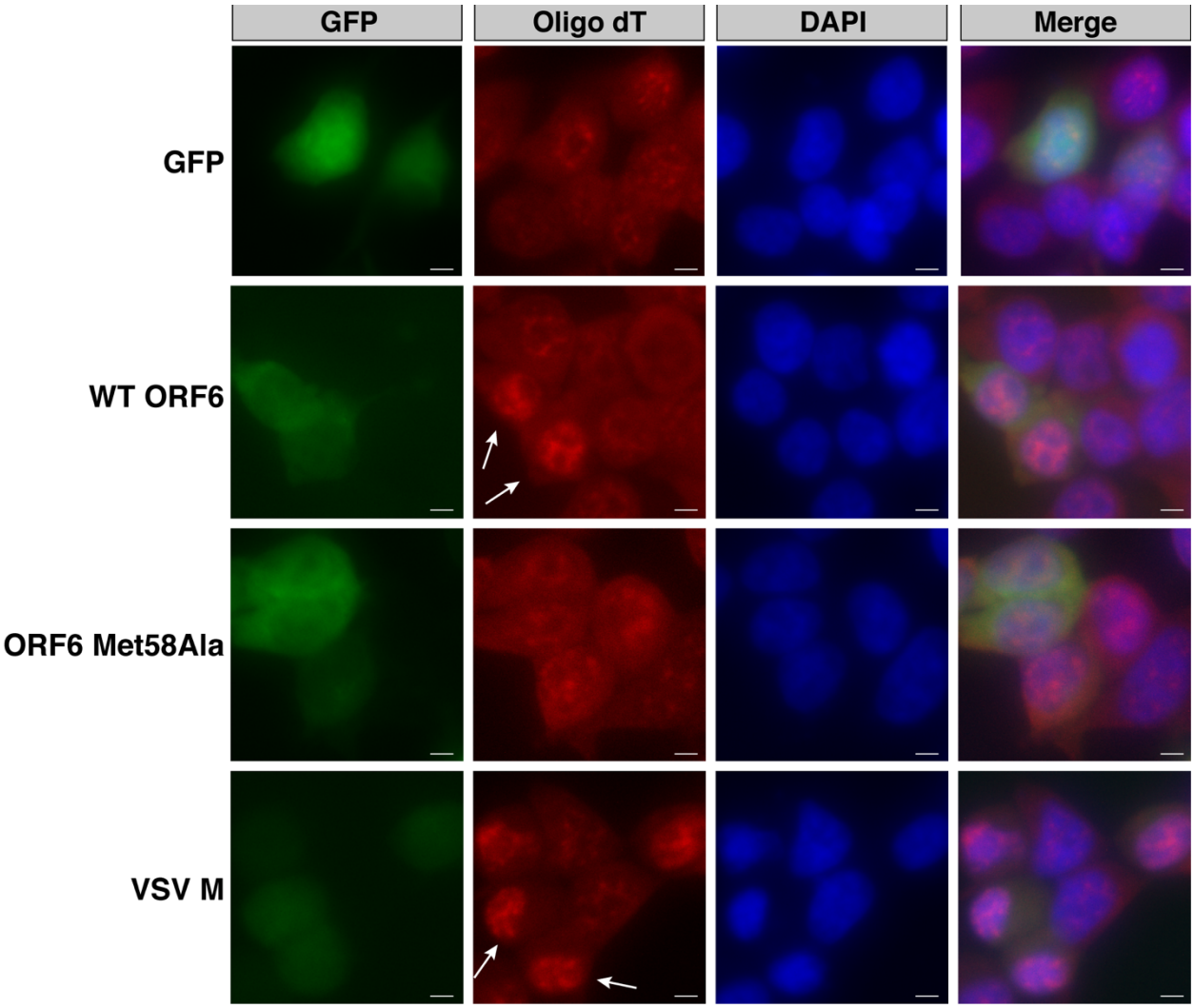

Figure 3. ORF6 causes mRNA to accumulate within the nucleus. 293T cells were transiently transfected with GFP-tagged constructs, incubated for 24 hours, and stained for GFP, poly-A mRNA, and DNA. mRNA in cells transfected with GFP or ORF6 Met58Ala was diffusely present throughout the cell. Cells transfected with ORF6 or VSV M showed an accumulation of mRNA within the nucleus (white arrows). Scale bar: 5 μm.

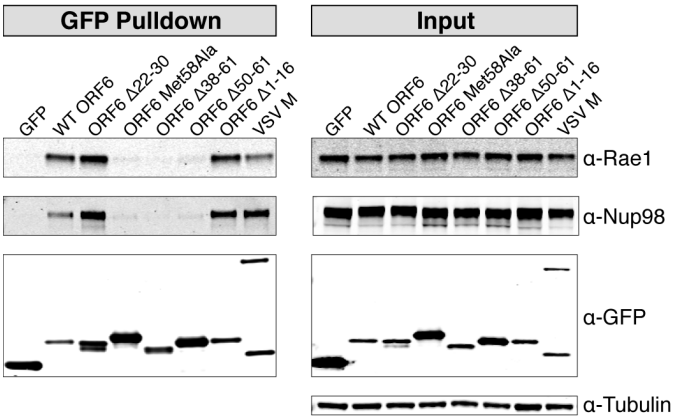

Figure 4. Affinity purification of GFP-tagged constructs. 293T were transiently transfected with GFP-tagged constructs. Forty-eight hours after transfection, the GFP-tagged proteins were rapidly captured using an anti-GFP resin. Western blotting revealed ORF6 interacts with the mRNA nuclear export factor Rae1 and the nuclear pore complex protein Nup98. ORF6 constructs with C-terminal deletions or a substitution did not pull down Rae1 or Nup98.

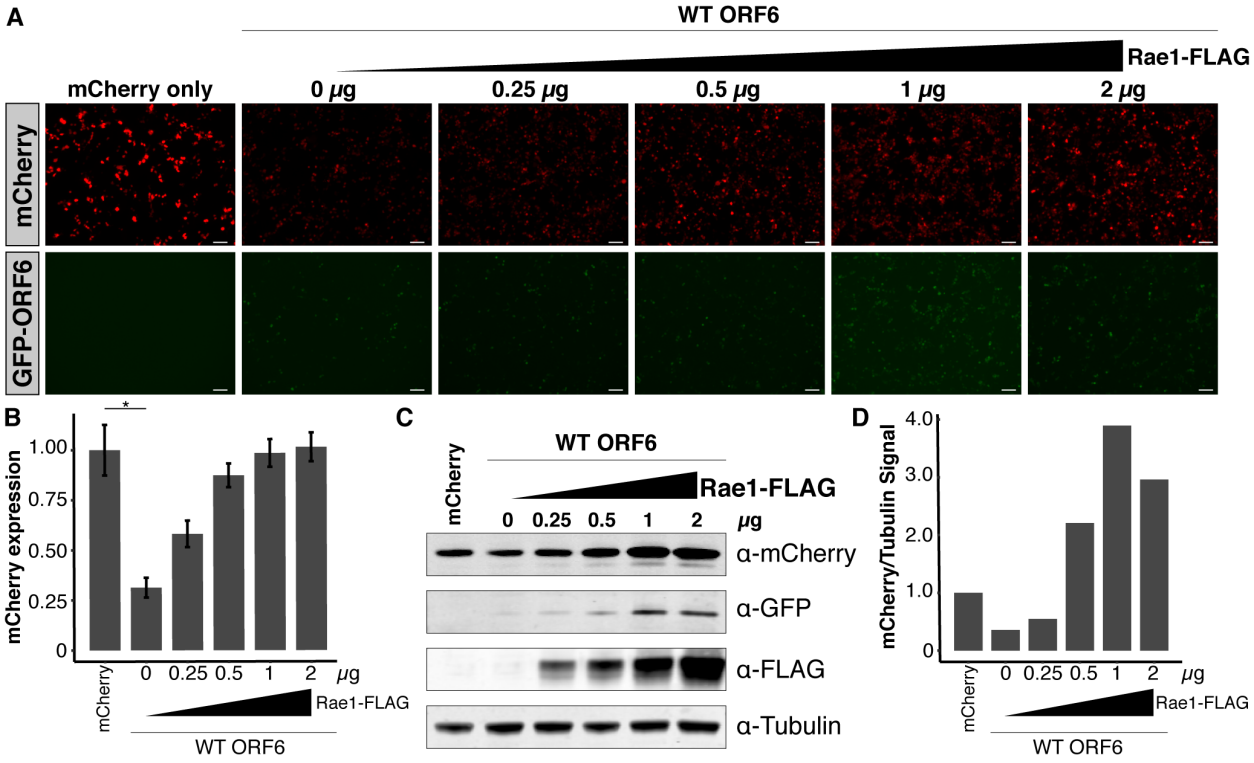

Figure 5. Overexpression of Rae1 rescues mCherry expression in cells transfected with ORF6. A) 293T cells were co-transfected with equal amounts GFP-ORF6 and mCherry and an increasing amount of Rae1. Expression of the fluorescent reporters was visualized and B) quantified 48 hours after transfection. In the presence of ORF6, mCherry expression was restored in a dose-dependent manner. C) Western blotting and D) densitometry confirmed mCherry expression was rescued in a dose-dependent manner with of increasing Rae1-FLAG. * $p < 0.05$. Scale bar: 100 μm.

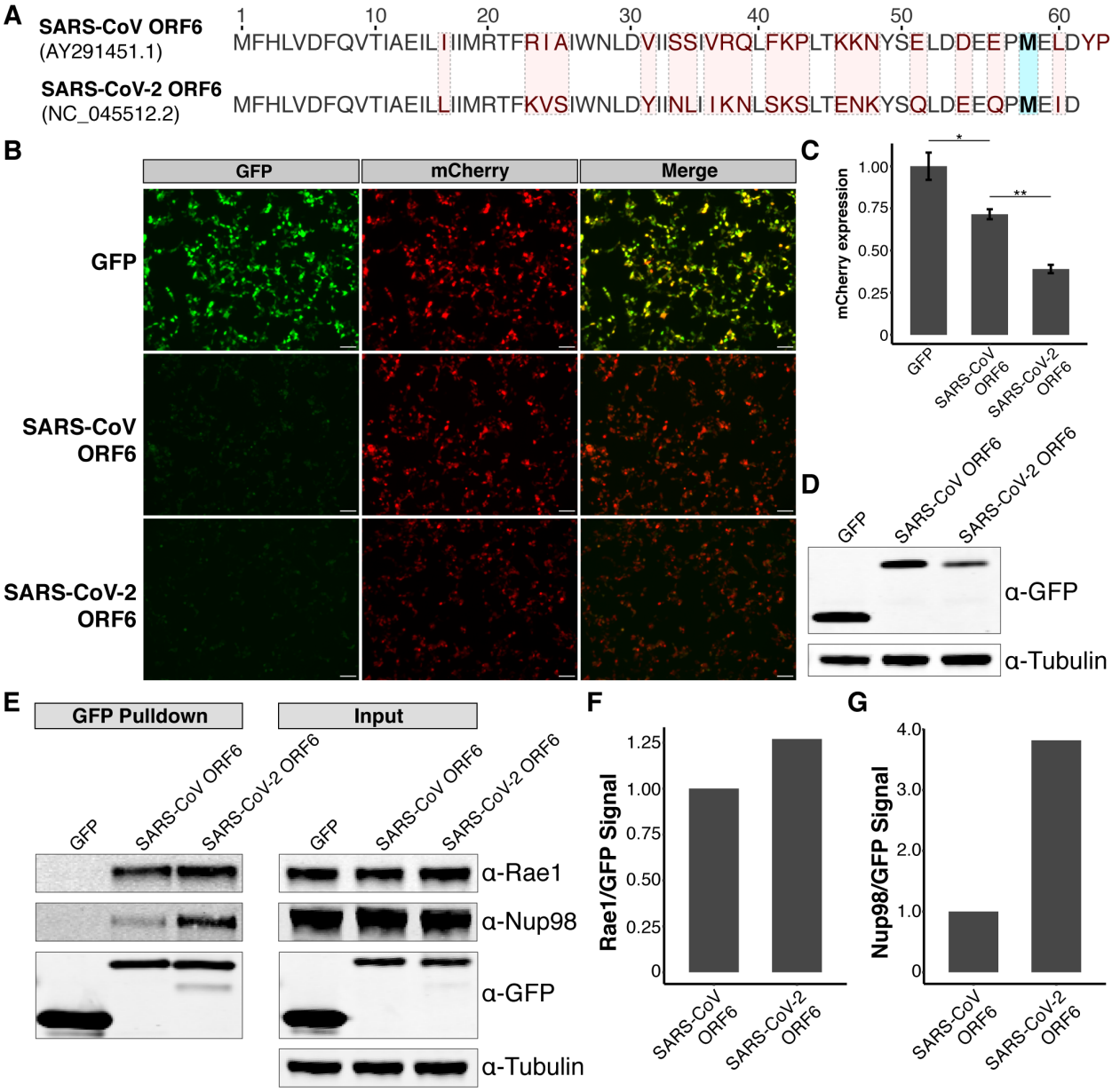

Figure 6. SARS-CoV-2 ORF6 represses reporter expression and copurifies with relatively more Rae1-Nup98 than SARS-CoV ORF6. A) Comparison between the amino acid sequences of ORF6 of SARS-CoV and ORF6 of SARS-CoV-2. Residues differing between the two viruses are highlighted in red. The residue (Met58) implicated in binding the Rae1•Nup98 complex is highlighted in blue. B) 293T were transiently transfected with GFP-tagged constructs and mCherry and visualized 24 hours after transfection. Cells transfected with SARS-CoV-2 ORF6 showed C) significantly reduced mCherry expression compared to those transfected with SARS-CoV ORF6. D) Western blotting showed decreased expression of SARS-CoV-2 ORF6 compared to SARS-CoV ORF6 in 293T cells. E) Affinity purification of GFP-tagged constructs demonstrates both ORF6 of SARS-CoV and ORF6 of SARS-CoV-2 interact with Rae1 and Nup98. Densitometry shows SARS-CoV-2 ORF6 copurifies with relatively more F) Rae1 and G) Nup98 compared SARS-CoV ORF6. * $p < 0.05$; ** $p < 0.01$. Scale bar: 100 μm.